Effect of the Metal on metal-based Disulfide/Thiolate Interconversion: Manganese versus Cobalt

Marcello Gennari, Deborah Brazzolotto, Shengying Yu, Jacques Pécaut, Christian Philouze, Mathieu Rouzières, Rodolphe Clérac, Maylis Orio, Carole Duboc

Effect of the metal on metal-based disulphide/thiolate interconversion: manganese *vs* cobalt.

Marcello Gennari,[a] Deborah Brazzolotto,[a] Shengying Yu,[a] Jacques Pécaut,[b] Christian Philouze,[a] Mathieu Rouzières,[d,e] Rodolphe Clérac,[d,e] Maylis Orio, Carole Duboc[a]

[a] *Univ. Grenoble Alpes, CNRS UMR 5250, DCM, F-38000 Grenoble, France.*
[b] *Univ. Grenoble Alpes, INAC-SCIB, F-38000 Grenoble, France CEA, INAC-SCIB, Reconnaissance Ionique et Chimie de Coordination, F-38000 Grenoble, France.*
[d] *CNRS, CRPP, UPR 8641, F-33600 Pessac, France.*
[e] *Univ. Bordeaux, CRPP, UPR 8641, F-33600 Pessac, France.*

Abstract

It has been recently proposed that disulphide/thiolate interconversion supported by transition metal ions is involved in several relevant biological processes. In this context, the present contribution represents a unique investigation on the effect of the nature of the metal (M) on the M^{n+}-disulphide / $M^{(n-1)+}$-thiolate switch properties. The new disulphide-bridged dinuclear Mn^{II} complex, **Mn^{II}_2SS**, like its isostructural Co^{II}-parent compound, **Co^{II}_2SS** (*Angew. Chem. Int. Ed.* **2014**, 53, 5318), can undergo a reversible M^{II} disulphide/ M^{III} thiolate interconversion mediated by iodide, leading to the first disulphide/ thiolate switch based on Mn. The **Mn^{II}_2SS** complex slowly reacts with Bu_4NI in CH_2Cl_2 to afford the mononuclear Mn^{III}-thiolate complex, **Mn^{III}I**. However, the process is much slower (~16 h) and much less efficient (~30% yield) with respect to the instantaneous and quantitative conversion of **Co^{II}_2SS** into **Co^{III}I** in similar conditions. Our arguments to rationalize this different behaviour are based on the electrochemical properties of the involved Co and Mn complexes and on the DFT-calculated energetics of the disulphide/thiolate conversion. Both Mn and Co systems are reversible: when iodide is removed with Ag^+, the **M^{II}_2SS** complexes are regenerated, still with a much slower reaction for Mn.

Introduction

Thiolate/disulphide redox conversion is implicated in various essential biological processes[1] including the folding and stability of most of the proteins. More importantly, it also plays a key role in the intracellular regulation by acting as a reversible switch that turns ON or OFF the reactivity of a protein. Different biological strategies are employed to precisely control the thiolate/disulphide balance; in particular, it has been recently proposed that metal ions, especially copper, can mediate thiolate/disulphide interconversion processes. Such copper-based systems seem to be implicated in the deliver of copper from the human Sco1 to the Cu_A site of the cytochrome c oxidase,[2] and in the protection of the cells against reactive oxygen species.[3]

On the other hand, the reactivity of disulphides or thiolates in the presence of a metal ion has attracted the attention of chemists as an interesting synthetic tool for the conception of functional materials and original metal-based molecular architectures.[4] Actually, the coordinating properties of sulfur display a remarkable versatility that can be employed for the synthesis of various molecular assemblies. In the presence of a metal, the disulphide atoms could (i) remain uncoordinated, (ii) be involved in weak interaction, or (iii) undergo a reductive cleavage of the S-S bond. In the last case, the resulting thiolates can act as terminal

or bridging ligands to generate many types of molecular inorganic auto-assemblages with controlled or infinite nuclearity.

In this context, the electronic and redox properties of the metallic complexes should be accurately fine-tuned to generate the targeted metal-sulphur motifs and/or to control the thiolate/disulphide equilibrium. Obviously, the nature of the metal should play a key role in the M^{n+}-disulphide/ $M^{(n-1)+}$-thiolate interconversion process. However, such investigation has never been reported so far, these molecular switches remaining rare and mainly limited to Cu^{I} disulphide/ Cu^{II} thiolate based systems.[5] Recently, we have reported the first example that does not contain copper, a Co-based switch based on a very clean, quantitative and reversible Co^{II} disulphide/ Co^{III} thiolate conversion mediated by chloride anions.[6] Extension to other transition metal ions is thus mandatory to better understand the impact of the metal on such processes.

Manganese is very attractive in this sense because a notable lower metal-sulphur affinity with respect to the late transition copper or cobalt metal ions is expected, as well as very distinctive electronic properties due to a decrease of the covalent character of the metal-sulphur bound from Cu^{II} to Mn^{II}. Moreover the reactivity of thiolates in the presence of Mn complexes has been only investigated in the case of the anionic $[Mn^{I}(CO)_3(SPhS)]^-$ (SPhS = 1,2 benzenedithiol), which is converted into a dinuclear $[Mn^{I}_2(CO)_6(SPhSSPhS)]$ in the presence of protons with the concomitant H_2 formation.[7]

Herein, we report on the synthesis and characterization of a new disulphide-bridged dinuclear Mn^{II} complex, $[Mn^{II}_2(LSSL)](PF_6)_2$ (**Mn^{II}_2SS**) (Scheme 1), isostructural to the previously reported Co^{II}-parent compound, $[Co^{II}_2(LSSL)](PF_6)_2$ (**Co^{II}_2SS**).[6] The reactivity of **Mn^{II}_2SS** with halide anions (in particular with iodide) has been investigated. As in the case of **Co^{II}_2SS**, coordination of the halide to metal induces disulphide/thiolate conversion. Even though the process occurs in a much less efficient way, it remains reversible. In combination with theoretical calculations, the reactivity of the cobalt and manganese switches is finally compared and discussed.

Experimental section

$[Mn^{II}_2(LS)(LSH)]ClO_4$ (**Mn^{II}_2SH**)[8] and $[Co^{II}_2(LSSL)](PF_6)_2$ (**Co^{II}_2SS**)[6] were prepared according to reported procedures. The syntheses/electrosyntheses of $[Mn^{II}_2(LSSL)](PF_6)_2$ (**Mn^{II}_2SS**) and $[Mn^{III}(LS)I]$ (**$Mn^{III}I$**) were performed under argon, while the corresponding work-up was carried out under air atmosphere. The infrared spectra were recorded on a

Magna-IR TM 550 Nicolet spectrometer as KBr pellets. The elemental analyses were carried out with a C, H, N analyzer (SCA, CNRS). The ESI-MS spectra were registered on a Bruker Esquire 3000 Plus ion trap spectrometer equipped with an electrospray ion source (ESI). The samples were analyzed in positive and negative ionization mode by direct perfusion in the ESI-MS interface (ESI capillary voltage= 2kV, sampling cone voltage= 40 V). The electronic absorption spectra were recorded on a Varian Cary 300 absorption spectrophotometer or on a MCS 501 UV-NIR (Carl Zeiss) photodiode-array spectrophotometer in quartz cells (optical path length: 0.5-1.0 cm).

Electrochemical measurements. Tetrabutylammonium hexafluorophosphate (NBu_4PF_6) was used as received and stored in glove box. Acetonitrile (99.9+ %, extra dry) and dichloromethane (99.99%) were degassed with argon prior to use. Electrochemical experiments were performed under argon, in a glove box with less than 5 ppm of O_2, by using a SP300 Bio-Logic potentiostat/galvanostat. A standard three-electrode electrochemical cell was used. Potentials were referred to an Ag/0.01 M $AgNO_3$ reference electrode in CH_3CN + 0.1 M Bu_4NClO_4 and measured potentials were calibrated through the use of an internal Fc/Fc^+ standard. The working electrode was a vitreous carbon disk (3 mm in diameter) polished with 2 μm diamond paste (Mecaprex Presi) for cyclic voltammetry (Ep_a, anodic peak potential; Ep_c, cathodic peak potential). Exhaustive electrolysis was carried out on reticulated vitreous carbon electrode 45 PPI (the electrosynthesis Co. Inc.) (1 cm^3). The auxiliary electrode was a Pt wire in CH_3CN + 0.1 M Bu_4NPF_6.

Electrosynthesis of $[Mn^{II}_2(LSSL)](PF_6)_2$ (***Mn^{II}_2SS***). In a standard three-electrode electrochemical cell, an exhaustive electrolysis was carried out at controlled potential (+0.05 V *vs* Fc/Fc^+) on a pale orange suspension of **Mn^{II}_2SH**·0.5$KClO_4$ (53.0 mg, 0.037 mmol) in MeCN 0.1 M Bu_4NPF_6 (6 ml). During the electrolysis the mixture turned deep orange, and the formation of a yellow precipitate was successively observed. The experiment was stopped when the current was seen to decay to about 5% of its initial value. Under these conditions, the charge passed reached 6.3 C (corresponding to 1.76 electrons for **Mn^{II}_2SH**). The resulting mixture was left to stand overnight and then stored at -18 °C for 8 h. The obtained solid was filtered and extracted with CH_2Cl_2 (a big excess). The volume was then reduced to ~20 ml, and few drops of MeCN were added. After slow diffusion of diethyl ether, X-ray suitable orange-yellow single crystals were obtained (28 mg, 0.017 mmol, 46%), corresponding to

Mn^{II}_2SS·$2CH_3CN$. IR (cm^{-1}): 3058 (w), 1598 (s), 1570 (m), 1491 (m), 1480 (m), 1465 (m), 1443 (s), 1287 (w), 1210 (w), 1187 (w), 1155 (w), 1087 (s br), 1022 (w), 1016 (w), 847 (vs), 754 (s), 743 (s), 697 (s), 558 (s, S-S stretching). ESI-MS ($5 \cdot 10^{-5}$ M, CH_2Cl_2, m/z, I%, M = $[Mn^{II}_2(LSSL)]$ unit): 633.2, 55 $[M]^{2+}$; 1311.3, 100 $[M(HCOO)]^+$ (positive ion mode); 1557.2, 25 $[M(PF_6)_2(H)]^-$; 1601.4, 80 $[M(PF_6)_2(HCOO)]^-$; 1655.2, 65 $[M(PF_6)_2(ClO_4)]^-$; 1701.2, 100 $[M(PF_6)_3]^-$ (negative ion mode). Anal. Calcd. for $C_{76}H_{60}F_{12}Mn_2N_4P_2S_4.0.5CH_3CN.4H_2O$ (1650.05): C, 56.05; H, 4.25; N, 3.82; Found: C, 56.20; H, 4.12; N, 3.73.

*Synthesis/electrosynthesis of $[Mn^{III}(LS)I]$ (**$Mn^{III}I$**)*. Bu_4NI (260 ml, 0.1 M solution in CH_2Cl_2, 0.026 mmol) was added to a yellow suspension of **Mn^{II}_2SS**·$2CH_3CN$ (19.0 mg, 0.012 mmol) in CH_2Cl_2 (5 ml) under stirring. After 40 hours, the resulting dark violet mixture was filtered to remove traces of unreacted **Mn^{II}_2SS**. After removing under vacuum the solvent from the filtrate, the resulting dark violet solid residue was washed with CH_3CN (3 ml) and dried. X-ray suitable dark violet crystals, corresponding to **$Mn^{III}I$**, were obtained by slow diffusion of diisopropyl ether onto a CH_2Cl_2 solution of the product (6.1 mg, 0.008 mmol, 33%). Alternatively, **$Mn^{III}I$** can be obtained in higher yields by carrying out the following procedure. In a standard three-electrode electrochemical cell, an exhaustive electrolysis was carried out at controlled potential (-0.60 V *vs* Fc/Fc^+) on a pale orange suspension of **Mn^{II}_2SH**·$0.5KClO_4$ (60.0 mg, 0.045 mmol) in MeCN 0.1 M Bu_4NPF_6 (7 ml), in the presence of Bu_4NI (188.1 mg, 0.509 mmol). During the electrolysis the mixture turned dark brown-violet, and the formation of a violet precipitate was successively observed. The experiment was stopped when the charge passed reached 9.5 C (corresponding to ~1.1 electrons for **Mn^{II}_2SH**). The obtained solid was filtered and extracted with CH_2Cl_2 (a big excess). The solvent was removed under vacuum and the resulting solid was washed with MeCN (2 × 5 ml), filtered, dried and collected as a dark violet powder (36.0 mg, 0.047 mmol, 52%), corresponding to **$Mn^{III}I$**. IR (cm^{-1}): 3046 (w), 2922 (m), 2852.70 (w), 2363 (w), 1598 (s), 1568 (m), 1484 (s), 1484 (m), 1466 (m), 1441 (s), 1421 (w), 1260 (m), 1183 (w), 1154 (w), 1080 (s br), 1017 (m), 743 (m), 693 (m), 597 (m). ESI-MS ($5 \cdot 10^{-5}$ M, CH_2Cl_2, m/z, I%, M = $[Mn^{III}(LS)]$ unit): 633.2, 100 $[M]^+$; 1002.3, 60 $[(Bu_4N)MI]^+$; 1393.2, 50 $[M_2I]^+$ (positive ion mode); 887.0, 100 $[MI_2]^-$; 1647.0, 50 $[M_2I_3]^-$ (negative ion mode). Anal. Calcd. for $C_{38}H_{30}MnN_2S_2I \cdot 0.1CH_2Cl_2$ (769.17): C, 59.49; H, 3.96; N, 3.64; Found: C, 59.39; H, 3.99; N, 3.82.

X-ray Crystallography. A summary of data collection and structure refinement for **Mn^{II}_2SS**·2CH_3CN and **Mn^{III}I** is reported in Table S1. Selected bond distances and angles are provided in Table 1. Single-crystal diffraction data for **Mn^{II}_2SS**·2CH_3CN were measured on an Oxford-Diffraction XCalibur diffractometer with a Sapphire 3 CCD detector (MoKα radiation, graphite monochromator, λ 0.71073Å) at 200 K. The CrysAlisPro program package (Agilent Technologies, Version 1.171.35.19) was used for cell refinements and data reductions. An absorption correction (CrysAlisPro) was applied to the data. Single-crystal diffraction data for **Mn^{III}I** were measured on an Bruker-AXS-Enraf-Nonius KappaCCD diffractometer with a CCD area detector (MoKα radiation, graphite monochromator, λ 0.71073Å) at 150 K. The OLEX2 program package was used for cell refinements and data reductions.[9] An absorption correction (SADABS) was applied to the data. For both complexes, the molecular structure was solved by direct methods and refined on F2 by full matrix least-squares techniques using SHELXTL package[10] and all non-hydrogen atoms were refined anisotropically. For **Mn^{II}_2SS**·2CH_3CN, all hydrogen atoms were found by Fourier transformation and refined with individual isotropic displacement parameters. For **Mn^{III}I**, all hydrogen atoms were placed at their calculated positions.

Magnetic measurements. Magnetic measurements were performed on a polycrystalline sample of **Mn^{II}_2SS**·2CH_3CN. The sample was sealed in a polyethylene bag (3 × 0.5 × 0.02 cm) in order to collect data in the temperature range of 1.8 to 300 K at 1000 Oe. Magnetic measurements were obtained with the use of a Quantum Design SQUID magnetometer MPMS-XL functioning between 1.8 and 400 K for direct-current (dc) applied fields ranging from -7 to +7 T. Prior to the experiment, the field-dependent magnetization was measured at 100 K on the sample in order to prove the absence of any bulk ferromagnetic impurities. On the other hand, when fitting the magnetic data, it was necessary to introduce in the magnetic model a paramagnetic Curie impurity that was assumed to be a mononuclear Mn^{II} species (S = 5/2). Its amount was estimated at 3.3(5)%. The magnetic data were corrected for the sample holder and diamagnetic contributions.

Commenté [MG1]: RODOLPHE, check STP

Computational details. All theoretical calculations were based on the Density Functional Theory (DFT) and were performed with the ORCA program package.1 Full geometry optimizations were carried out for all complexes using the hybrid functional B3LYP2-4 in

combination with the TZV/P5 basis set for all atoms and by taking advantage of the resolution of the identity (RI) approximation in the Split-RI-J variant6 with the appropriate Coulomb fitting sets.7 Increased integration grids (Grid4 in ORCA convention) and tight SCF convergence criteria were used. Vibrational frequency calculations were performed to ensure that each geometry optimization converged to a real minimum. Solvent effects were accounted for according to the experimental conditions. For that purpose, we used the acetonitrile solvent (ε= 9.08) within the framework of the conductor like screening (COSMO) dielectric continuum approach.8 The relative energies were obtained from single-point calculations using the B3LYP9,10functional together with the TZV/P basis set. They were computed from the gas-phase optimized structures as a sum of electronic energy, thermal corrections to free energy, and free energy of solvation. The Heisenberg isotropic exchange coupling constants J were evaluated from single point calculations based on the Broken Symmetry (BS) approach11-13 using the B3LYP functional and the TZV/P basis set. The Yamaguchi formula14,15 was used to estimate the exchange coupling constants J based on the Heisenberg–Dirac–van Vleck Hamiltonian: H = –2JS1S2.16-19

Mis en forme : Couleur de police : Rouge

Results and Discussion

The $[Mn^{II}_2(LSSL)](PF_6)_2$ complex (**Mn^{II}_2SS**, Scheme 1) has been obtained from the oxidative electrolysis of the $[Mn^{II}_2(LS)(LSH)]ClO_4$ complex (**Mn^{II}_2SH**), which contains a bound thiol on one of the Mn^{II} ions (MeCN at E = +0.05 V vs Fc^+/Fc). We have previously reported that the cyclic voltammogram (CV) of **Mn^{II}_2SH** displays an irreversible anodic peak at Ep_a = -0.01 V, assigned to a two-electron metal based oxidation.[8] The corresponding cathodic potential (Ep_c = -0.47 V) is consistent with a fast chemical rearrangement associated with the deprotonation of the thiol group to lead to $[Mn^{III}_2(LS)_2](PF_6)_2$ (**Mn^{III}_2**, Scheme 1). Coherently, during the oxidative electrolysis of **Mn^{II}_2SH**, the colour of the solution turns from light orange to deep orange, which corresponds to the formation of **Mn^{III}_2**. However, this deep orange solution evolves to a light yellow solution with time. This final species has been isolated and identified as **Mn^{II}_2SS**, an isoelectronic form of **Mn^{III}_2**, by X-ray diffraction. In analogy to the previously reported Co isostructural complex $[Co^{II}_2(LSSL)](PF_6)_2$ (**Co^{II}_2SS**), **Mn^{II}_2SS** reacts with halides (X=Cl, Br, I) in CH_2Cl_2 (see Scheme 1) to afford mononuclear Mn^{III} $[Mn^{III}(LS)X]$ (**$Mn^{III}X$**) complexes. Here, we report on the case of X=I, as the most stable complex among the series is the dark violet **$Mn^{III}I$** species, which has been structurally characterized. The Mn^{II}_2-disulphide / Mn^{III}-thiolate conversion process, mediated by the

iodide anion, will be analysed in the following sections, and it will be discussed in comparison with the corresponding Co^{II}_2-disulphide / Co^{III}-thiolate system.

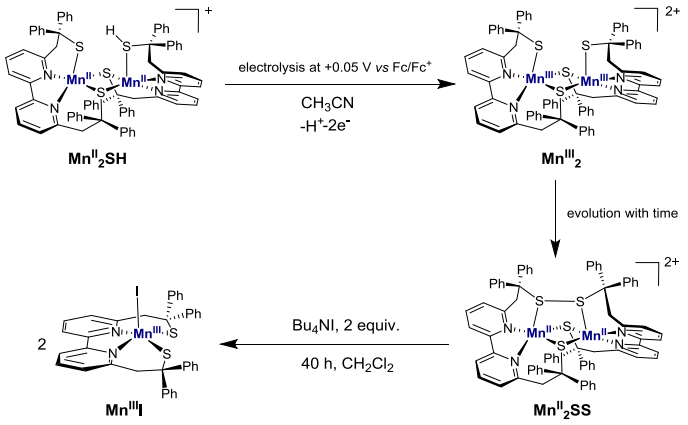

Scheme 1

Structural properties

The X-ray structures of **Mn^{II}_2SS** and **Mn^{III}I** are shown in Figure 1, and selected bond distances and angles are collected in Table 1.

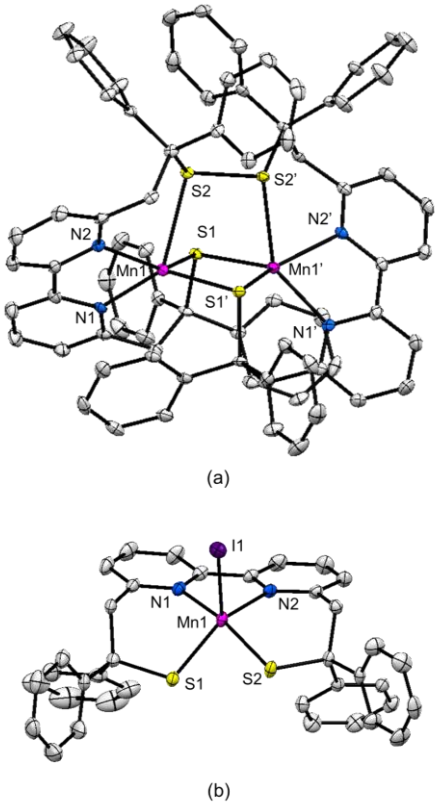

Figure 1. Molecular structures of (a) $\mathbf{Mn^{II}_2SS}\cdot 2CH_3CN$, (b) $\mathbf{Mn^{III}I}$. The thermal ellipsoids are drawn at 30% probability level. All hydrogen atoms, counteranions and solvent molecules are omitted for clarity.

The $\mathbf{Mn^{II}_2SS}$ complex (see Figure 1a) consists in a μ-1,2-dimercapto-bridged dinuclear Mn^{II} complex containing a rare $\{Mn_2S_2(SS)\}$ core that has been previously found only in two dinuclear Mn^{I} complexes.[7, 11] The complex is isostructural to the previously described Co^{II}-parent compound, $\mathbf{Co^{II}_2SS}$, displaying the same symmetry (space group C2/c).[6] As in the case of $\mathbf{Co^{II}_2SS}$, the disulphide remains coordinated to the Mn^{II} ions despite the fact that only a weak interaction is expected between a disulphide and d^5 Mn^{II} ions. The $\{Mn_2S_2\}$ plane is quasi planar (deviation from the S1Mn1S1'Mn1' plane: less than 0.059 Å, angle between the S1Mn1S1' and S1Mn1'S1' planes of 8.53°). The Mn sites are equivalent because of a C_2 symmetry axis, which is orthogonal to the average $\{Mn_2S_2\}$ plane. The manganese ions are not involved in a direct metal-metal interaction as the Mn…Mn distance is too long

(3.1469(10) Å). Each manganese ion is penta-coordinated surrounded by an N2S3 donor set in a distorted square pyramidal geometry with a τ_5 value of 0.07 for each Mn.[12] While the plane is defined with the four donor-atoms of one LS unit of LSSL, the axial position is occupied by the $S_{thiolate}$ atom of the second LS unit. A larger distortion from the square pyramidal geometry is observed in the isostructural Co complex with a τ_5 value of 0.13 for each Co ion. **Mn^{II}_2SS** displays similar structural properties than those of **Mn^{II}_2SH** except the fact that the terminal Mn-bound sulfurs have been oxidized into a disulphide bridge in **Mn^{II}_2SS**. Indeed, the short S2-S2' distance of 2.0357(17) Å is typical of a disulphide bond and is remarkably shorter than in the reported complexes with a $\{Mn^{I}_2S_2(SS)\}$ core (between 2.206 Å and 2.224 Å).[7, 11] The Mn1(1')-S2(2') bond lengths (2.6947(10) Å) are comparable to those of the Mn-S(H) bond found in **Mn^{II}_2SH** (2.6462(10) Å). In addition, all metal-ligands distances are slightly longer in the Mn derivate (in the range 8 pm - 16 pm) in comparison with the Co analogue, consistent with the periodic trend, as well as the S-S bond (2.0357(17) Å vs 2.0243(13) Å in the Co complex). To the best of our knowledge, **Mn^{II}_2SS** is the first reported complex containing a Mn^{II}-coordinated disulphide bridge (Mn^{II}-(R)SS(R)-Mn^{II}, R=alkyl or aryl), such structural motifs being found only in a few carbonyl disulphide Mn^{I}_2 complexes.[7, 11, 13]

The X-ray structure of the mononuclear **Mn^{III}I** complex (see Figure 1b) shows that the Mn^{III} ion is penta-coordinated, centred around a distorted square pyramidal N_2S_2I coordination sphere with the two N and two S atoms of the LS^{2-} ligand located in the equatorial plane and the I^- ion occupying the axial position. Mononuclear penta-coordinated Mn^{III} complexes are quite uncommon, and mainly obtained in the presence of salen,[14] porphyrin[15] or cyclam[16] supporting ligands. The **Mn^{III}I** complex is isostructural to the previously described Co^{III} parent **Co^{III}I**,[6] displaying the same symmetry (space group P21/c). The Mn^{III} ion is shifted approximately 0.489 Å from the mean N_2S_2 plane toward the axial I ligand, slightly more than in the case of the Co analogue (0.435 Å). The Co-N bond distances are shorter than those in **Mn^{II}_2SS**, consistent with the difference of the ionic radii for Mn^{II} and Mn^{III}. The valency angles of the equatorial N_2S_2 plane evidence strong distortions in the plane as attested by the S1-Mn-N2 and S2-Mn-N1 angles of 144.21(12)° and 163.31(13)°. The corresponding τ_5 value[12] is 0.318, consistent with a slightly less distorted square pyramidal geometry with respect to the isostructural **Co^{III}I** complex (τ_5 =0.332).

Magnetic properties

Variable-temperature magnetic susceptibility data were collected on a powdered sample of **Mn^{II}_2SS** in the 1.8-300 K temperature range at 1000 Oe (Figure 2).

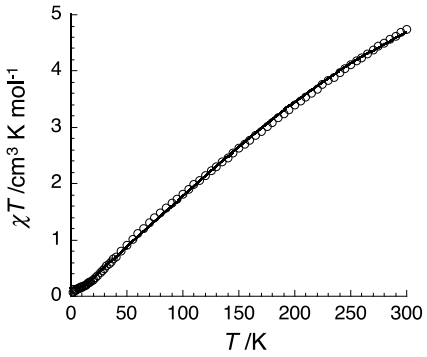

Figure 2. Temperature dependence of the χT product (where χ is the molar magnetic susceptibility equal to M/H per complex) measured at 1000 Oe for **Mn^{II}_2SS**.

The steadily decrease of χT product to nearly zero at 2 K suggests the presence of significant antiferromagnetic exchange occurring in the complex, as in the case of the Co analogue, **Co^{II}_2SS**. Therefore, the magnetic data were analysed by an isotropical spin-dimer Heisenberg model $H = -2JS_AS_B$, assuming that the two metallic ions are high spin Mn^{II} (S_A=S_B=5/2). The resulting best fit for **Mn^{II}_2SS** affords S=0, g_A=g_B=2.02(5) and J=-17(2) cm^{-1}. This value is in agreement with the calculated J value (J^{calc}=-23.52 cm^{-1}) for the optimized $[Mn^{II}_2(LSSL)]^{2+}$ complex (see Figure S3 and computational details). A molar fraction of paramagnetic impurity, assumed to be mononuclear (S=5/2), of 3.3(5)% has been added. The bridging thiolate ligands mediate an antiferromagnetic exchange interaction between the two Mn^{II} centres leading to a diamagnetic S=0 ground spin state. The magnetic coupling between two Mn^{II} ions is generally low in magnitude (less than 15 cm^{-1}). [17] In the literature the number of polynuclear Mn^{II} complexes with thiolate bridge(s) is limited and, to the best of our knowledge, the magnetic properties have been reported only for one of those, *i.e.* a linear trinuclear Mn^{II} complexes with a mono μ-thiolato bridge between each Mn ion (J=-9.8 cm^{-1}).[18] The stronger antiferromagnetic coupling found in **Mn^{II}_2SH** and **Mn^{II}_2SS** can be attributed to the quasi-planarity of their $\{Mn_2S_2\}$ core that allows orbital overlap. This is consistent with the observed decrease in the J magnitude from **Mn^{II}_2SH** (J=-22 (1) cm^{-1}) to **Mn^{II}_2SS**. Indeed, the $\{Mn_2S_2\}$ core in **Mn^{II}_2SS** presents larger deviation from planarity than

Mis en forme : Non Exposant/ Indice

Mis en forme : Non Exposant/ Indice

Mis en forme : Police :Italique

Mis en forme : Police :Non Italique, Exposant

that in **Mn^{II}_2SH** (deviation from the S2Mn1S52Mn2 plane: less than 0.017 Å, angle between the S2Mn1S52 and S2Mn2S52 planes of 2.36°).

Reactivity with iodide: disulphide-thiolate interconversion

The reaction of the Mn^{II}–disulphide complex **Mn^{II}_2SS** with Bu_4NI gives a more stable Mn^{III}-thiolate adduct, **$Mn^{III}I$**, with respect to the chloride and bromide derivates. We have thus thoroughly investigated this iodide-induced intramolecular redox process by UV-Vis absorption (Figure 3), and compared it to the corresponding **Co^{II}_2SS/$Co^{III}I$** system (Figure 4).

At 20 °C, the **Mn^{II}_2SS** complex (clear yellow solution) slowly reacts with Bu_4NI (2.5 eq.) in CH_2Cl_2 under argon to afford the **$Mn^{III}I$** complex (dark violet solution). The formation of **$Mn^{III}I$** is evidenced by the progressive increase in the absorbance of a visible band at 550 nm, a maximum amount of product being obtained after approximately 16 hours. **$Mn^{III}I$** is generated only in a ~30% yield, based on the epsilon value of **$Mn^{III}I$** at 550 nm (~2250 $M^{-1}cm^{-1}$) determined from the isolated product. The homologous process involving the **Co^{II}_2SS** complex, isostructural to **Mn^{II}_2SS**, is much more efficient. Under comparable conditions (2.0 eq. of Bu_4NI in CH_2Cl_2 at 20 °C), the clear yellow solution of the **Co^{II}_2SS** is converted immediately and quantitatively into a dark brown solution containing Co^{III} iodide species, in analogy to what happens to **Co^{II}_2SS** in the presence of chlorides.[6] However, with X = I, it should be noted that partial aggregation of **$Co^{III}I$** is observed in solution (*vide infra*).

The further step was the investigation of the backward process *i.e.* the possibility to regenerate the initial **M^{II}_2SS** complex (M=Mn, Co) by removing of the iodide anion from **$M^{III}I$** *via* its reaction with $AgBF_4$. For both Mn and Co, the process is completely reversible, as the addition of a stoichiometric amount of $AgBF_4$ is sufficient to quantitatively regenerate the corresponding **M^{II}_2SS** dinuclear complex. This is attested by the complete disappearance of any feature typical of M^{III} ions in the respective final visible spectra and by the concomitant appearance of a vibration at ~558 cm^{-1} in both infrared spectra assigned to the S-S vibrational stretching mode of **M^{II}_2SS** (see Supporting Information). However, while the conversion of **$Co^{III}I$** into **Co^{II}_2SS** is direct and instantaneous, it is not the case for **$Mn^{III}I$**. In the conditions of Figure 3, the addition of $AgBF_4$ to a solution of **$Mn^{III}I$** leads to its conversion into a deep orange solution with a broad absorption band at ~475 nm in less than 5 seconds (step 2, Figure 3). This species corresponds to the previously described bis μ-thiolato dinuclear Mn^{III} complex with two terminal thiolate groups, **Mn^{III}_2** (see Scheme 1).[8] Then,

Mn^{III}_2 evolves in less than 6 minutes to its isoelectronic form, the **Mn^{II}_2SS** dimer (step 3, Figure 3), to fully complete the thiolate/disulphide cycle.

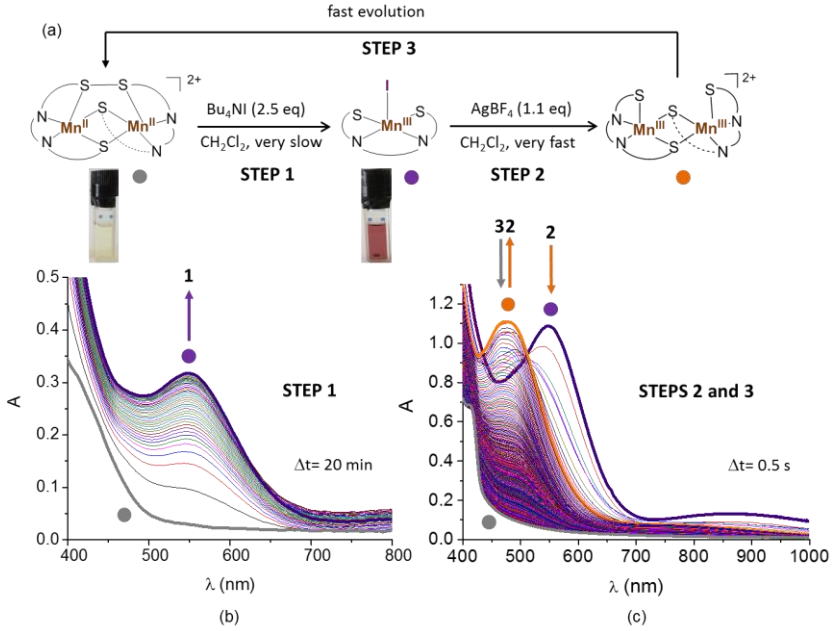

Figure 3. UV-Vis spectral evolution of: (b) a **Mn^{II}_2SS** solution (0.5 mM) in CH_2Cl_2 after the addition of Bu_4NI (2.5 eq) to afford **Mn^{III}I** (0.5 cm path length); (c) a **Mn^{III}I** solution (0.5 mM) in CH_2Cl_2 after the addition of $AgBF_4$ (1.1 eq, 0.1 M in MeCN), to recover **Mn^{II}_2SS** (1.0 cm path length). The experimental data are rationalized in (a).

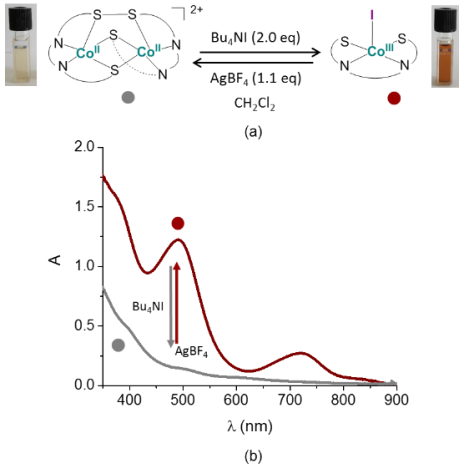

Figure 4. (b) UV-visible absorption spectra of **Co^{II}_2SS** (0.1 mM in CH_2Cl_2, 1.0 cm path length) recorded before (—) and (—) after the addition of Bu_4NI (2.0 eq), affording **Co^{III}I** immediately and quantitatively. The complete reversibility of the process is attested by the subsequent addition of $AgBF_4$ (1.1 equiv., 0.1 M in MeCN). The experimental data are rationalized in (a).

Electrochemical properties

The reduction properties of the different complexes have been investigated by cyclic voltammetry (CV, Figure 5 and Table 2) in order to get insights on the feasibility of the M^{III}-thiolate/M^{II}-disulphide interconversion to occur for both the **Mn^{II}_2SS/Mn^{III}I** and **Co^{II}_2SS/Co^{III}I** systems.

The CV of **Mn^{II}_2SS** displays an irreversible cathodic peak located at Ep_c = -1.17 V *vs* Fc^+/Fc. This signal can be attributed to the two-electron reduction of the disulphide bridge. Note that in the CV recorded immediately after addition of Bu_4NI (2.5 eq) to **Mn^{II}_2SS**, thus before its evolution into **Mn^{III}I**, the Ep_c value remains unchanged suggesting that the coordination of iodide(s) to Mn^{II} has a negligible effect on the redox stability of the S-S bridge.

Remarkably, the disulphide/thiolate redox system for the homologous **Co^{II}_2SS** complex is shifted of 430 mV more positively (Ep_c = -0.74 V),[6] when compared to **Mn^{II}_2SS**. This implies a remarkable impact of the nature of the metal ion on the redox stability of the disulphide, the disulphide form being more stabilized when coordinated to Mn^{II} than to Co^{II}.

The CVs of both **M^{III}I** complexes display an irreversible metal-based reduction process. The CV of **Mn^{III}I** displays an irreversible cathodic peak located at Ep_c = -0.68 V, promptly assigned to a one-electron $Mn^{III} \rightarrow Mn^{II}$ reduction. The anodic peak located at Ep_a = -0.04 V in the backward process is attributed to the oxidation of iodide released after the $Mn^{III} \rightarrow Mn^{II}$ reduction. The CV of **Co^{III}I** is more complicated. In this case, two reduction systems are observed, one at Ep_c = -0.66 V and one at Ep_c = -0.74 V. The ratio between the intensities of these two peaks varies with the concentration of complex, the first one slightly increasing under dilution. This is consistent with the presence of two species of different nuclearities in equilibrium, when **Co^{III}I** is dissolved in CH_2Cl_2. In this respect, two alternative equilibriums can be proposed:

i) $2[Co^{III}(LS)I] = [Co^{II}_2(LSSL)]^{2+} + 2I^-$

ii) $2[Co^{III}(LS)I] = [Co^{III}_2(LS)_2I]^+ + I^- = [Co^{III}_2(LS)_2I_2]$

The first possibility can be excluded as two equivalents of Bu_4NI are enough to fully convert $[Co^{II}_2(LSSL)]^{2+}$ into $[Co^{III}(LS)I]$. On the other hand, the second hypothesis is consistent with both the spectroscopic and redox properties of **Co^{III}I**. The peaks in the CV at Ep_c = -0.66 V

can be assigned to the one electron reduction process of [Co^{III}(LS)I] and that at Ep_c = -0.74 V to the proposed [Co^{III}_2(LS)$_2$I]$^+$ and/or [Co^{III}_2(LS)$_2I_2$ species.

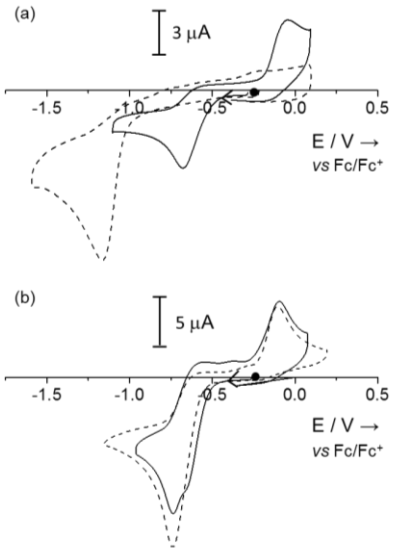

Figure 5. CVs of CH_2Cl_2 solutions (0.1 M Bu_4NPF_6) of (a) **Mn^{II}_2SS** (---, 0.5 mM) and **Mn^{III}I** (—, 0.4 mM), compared to (b) the CVs of **Co^{II}_2SS** (---, 0.85 mM) and **Co^{III}I** (—, 1.4 mM). Glassy carbon working electrode (3 mm diameter), scan rate of 100 mV·s^{-1}.

Theoretical calculations

DFT calculations were performed as a further contribution in the attempt to rationalize the different behaviour of the Co and Mn systems for M^{II}_2-disulphide/M^{III}-thiolate conversion. Geometry optimizations (see computational details) were performed both on the [M^{II}_2(LSSL)]$^{2+}$ dinuclear complexes and on the corresponding monomers obtained by breaking the S-S bond, [M^{III}(LS)]$^+$ (Figure S3). The resulting optimized geometries of [Mn^{II}_2(LSSL)]$^{2+}$ and [Co^{II}_2(LSSL)]$^{2+}$ compare well with the crystallographic data (maximum discrepancy of 0.12 Å and 0.16 Å[6] for coordination distances in the Mn and Co complexes, respectively), thus validating our computational approach. Regarding the optimized theoretical monomers, Loedwin spin populations (Table S2) are in the +1.82/+4.05 range for the metal centre and in the +0.09/-0.03 range for the sulphur atoms. The low radical character of the sulphurs with respect to that of the metal, also confirmed by the relatively low sulphur

character of the SOMOs (Figure S4), is consistent with M^{III}-thiolate complexes. Therefore, the Gibbs free energy (ΔG^0 at 0 K) of the reaction in Equation 1 can be considered as a rough estimation of the driving force for M^{II}_2-disulphide/M^{III}-thiolate conversion.

$$[M^{II}_2(LSSL)]^{2+} = 2[M^{III}(LS)]^{+} \qquad \text{(Equation 1)}$$

The computed values of ΔG^0 (0 K) are reported in Table 3, both in the gas-phase and in solution (CH_2Cl_2 medium) for M = Mn, Co. The dissociation of the Co^{II}_2-disulphide into two Co^{III}-thiolate units is highly exergonic (ΔG^0 = -15.1 kcal·mol^{-1} in CH_2Cl_2). The relative high stability of the monomeric $[Co^{III}(LS)]$ complex with respect to the corresponding $[Co^{II}_2(LSSL)]^{2+}$ dinuclear complex is in perfect agreement with the easy and efficient Co^{II}_2-disulphide/ Co^{III}-thiolate conversion experimentally observed. Conversely, the computed ΔG^0 for the parent Mn system is positive (ΔG^0 = +7.9 kcal·mol^{-1} in CH_2Cl_2), in accordance with the low reactivity of the Mn-based system. The iodide coordination to the Mn^{III} ion should stabilize enough the mononuclear species to allow the process to occur.

Concluding Remarks

In this work, we reported on the first example of a reversible disulphide/thiolate interconversion mediates by manganese ions. As for the parent cobalt switch, coordination (decoordination) to the metal ions of iodide induces disulphide to thiolate (thiolate to disulphide) conversion with concomitant metal oxidation (reduction). For both Mn and Co systems, the reversibility of the process seems to be favoured by the fact that the disulphido bridge remains coordinated to the metal centres in $\mathbf{M^{II}_2SS}$.

The conversion of $\mathbf{Mn^{II}_2SS}$ into $\mathbf{Mn^{III}I}$ mediated by iodide is notably less efficient (it occurs in a few minutes and partially) when compared with the corresponding cobalt-based system ($\mathbf{Co^{II}_2SS/Co^{III}I}$), which is quantitative and instantaneous. The backward reaction, initiated by removing the bound iodides, is also slower in the case of Mn. Indeed, the Mn^{II}_2-disulphide complex is not directly regenerated as for $\mathbf{Co^{II}_2SS}$, but arises from evolution of its isoelectronic $\mathbf{Mn^{III}_2}$ form.

Due to the high structural similarity of the dinuclear Mn and Co complexes, the difference in reactivity (disulphide to thiolate conversion) between them should be related to their electronic and/or redox properties. With this respect, we have analysed and compared i) the electrochemical cathodic (Ep_c) potential values for the $\mathbf{M^{II}_2SS}$ and $\mathbf{M^{III}I}$ species (Table 2) and ii) the calculated dissociation energies of the M^{II}_2-disulphide complexes into the corresponding M^{III}-thiolate monomers (Equations 1-2). The cathodic peak of $\mathbf{M^{II}_2SS}$ can be

attributed to the reduction of the S-S bridge, while that of **M^{III}I** to the reduction of the metal (from M^{III} to M^{II}). Although the Ep_c values don't contain direct thermodynamic information on the system (lack of redox reversibility), they give an indication on the feasibility of the internal redox process. In particular, in order to achieve reversible disulphide/thiolate interconversion, the Ep_c values of the LSSL/$2LS^-$ and M^{III}/M^{II} redox couples should be close enough to allow small structural modifications to address the direction of the internal electron transfer between the ligand and the metal. It is the case for the **Co^{II}_2SS/Co^{III}I** pair (see Table 2), resulting in an efficient switchable system. The coordination of iodide decreases the redox potential of the Co^{III}/Co^{II} couple so that the Co^{II} ions become enough reducing to reduce the disulphide into thiolates. Conversely, the redox potential of the LSSL/$2LS^-$ couple for the Mn-based system is surprisingly much lower than for the Co-based one (-1.17 V and –0.74 V, respectively). Consequently, coordination of iodide might not decrease enough the redox potential of the Mn^{III}/Mn^{II} couple: as a result, the disulphide/thiolate conversion can't occur efficiently.

Dissociation energies of the M^{II}_2-disulphide complexes into the corresponding M^{III}-thiolate monomers calculated by DFT methods confirm the same tendency. The process is slightly exothermic for the Co system (-15.1 kcal·mol^{-1} in CH_2Cl_2), while it becomes endothermic for the Mn system (+7.9 kcal·mol^{-1} in CH_2Cl_2), confirming the higher stability of the disulphide bridge in **Mn^{II}_2SS** with respect to the Co analogue. The conversion of **Mn^{II}_2SS** to **Mn^{III}I** with such unfavourable thermodynamics can be explained by the fact that the iodide coordination to the Mn^{III}-thiolate fragment strongly stabilizes **Mn^{III}I**.

In conclusion, this work represents an original contribution to improve the understanding of how the electronic and redox properties of the metal should be perfectly fine-tuned to allow a disulphide/thiolate conversion mediated by a metal to occur efficiently.

TOC

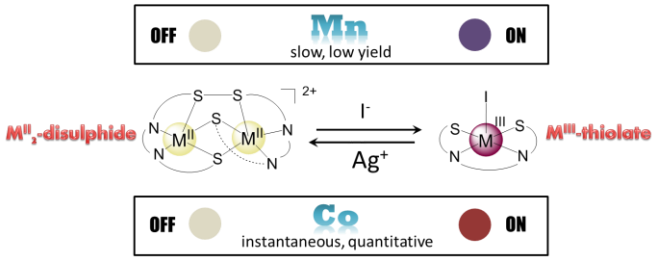

Acknowledgements. The authors gratefully acknowledge research support of this work by the French National Agency for Research n° ANR-09-JCJC-0087, Labex arcane (ANR-11-LABX-003) and COST Action CM1305 ECOSTBio (Explicit Control Over Spin-States in Technology and Biochemistry).

Table 1. Selected bond lengths (Å) and angles (°) for $\mathbf{Mn^{II}_2SS}\cdot 2CH_3CN$ and $\mathbf{Mn^{III}I}$.

$\mathbf{Mn_2SS}\cdot 2CH_3CN$		**MnI**	
Mn(1)-N(1)	2.151(3)	Mn(1)-N(1)	2.059(4)
Mn(1)-N(2)	2.194(3)	Mn(1)-N(2)	2.091(4)
Mn(1)-S(1)	2.4940(10)	Mn(1)-S(1)	2.2792(16)
Mn(1)-S(2)	2.6947(10)	Mn(1)-S(2)	2.2846(15)
Mn(1)-S(1)'	2.4340(9)	Mn(1)-I(1)	2.7450(12)
Mn(1)-Mn(1)'	3.1469(10)		
S(2)-S(2)'	2.0357(17)		
N(1)-Mn(1)-N(2)	76.43(10)	N(1)-Mn(1)-N(2)	79.25(16)
N(1)-Mn(1)-S(1)	88.66(7)	N(1)-Mn(1)-S(1)	92.26(13)
N(1)-Mn(1)-S(2)	132.99(7)	N(1)-Mn(1)-S(2)	163.31(13)
N(1)-Mn(1)-S(1)'	137.67(7)	N(1)-Mn(1)-I(1)	95.98(12)
N(2)-Mn(1)-S(1)	137.23(7)	N(2)-Mn(1)-S(1)	144.21(12)
N(2)-Mn(1)-S(2)	81.74(7)	N(2)-Mn(1)-S(2)	97.60(11)
N(2)-Mn(1)-S(1)'	117.72(8)	N(2)-Mn(1)-I(1)	99.56(11)
S(1)-Mn(1)-S(2)	79.90(3)	S(1)-Mn(1)-S(2)	80.69(6)
S(1)-Mn(1)-S(1)'	100.37(3)	S(1)-Mn(1)-I(1)	115.96(5)
S(2)-Mn(1)-S(1)'	89.33(3)	S(2)-Mn(1)-I(1)	100.71(5)
Mn(1)-S(1)-Mn(1)'	79.36(3)		

Table 2. Cathodic peak potentials (Ep_c) for the $\mathbf{M^{II}_2SS}$ and $\mathbf{M^{III}I}$ complexes (M = Mn, Co), as determined from the corresponding CVs in CH_2Cl_2, 0.1 M Bu_4NPF_6. The anodic peak potentials (Ep_a) of the corresponding backward processes are also shown.

	Ep_c (Ep_a)
$\mathbf{Mn^{II}_2SS}$	-1.17 (-)
$\mathbf{Co^{II}_2SS}$	-0.74 (-0.10)[6]
$\mathbf{Mn^{III}I}$	-0.68 (-0.04)
$\mathbf{Co^{III}I}$	-0.66, -0.74 (-0.10)

Table 3. Gibbs free energies (ΔG^0), computed at 0 K, for the reaction(s) in Equation 1, both in the gas-phase and in CH_2Cl_2 solution.

	ΔG in vacuum (kcal·mol^{-1})	*ΔG in CH_2Cl_2* (kcal·mol^{-1})
$[Mn^{II}_2(LSSL)]^{2+} = 2[Mn^{III}(LS)]^{+}$	+3.6	+7.9
$[Co^{II}_2(LSSL)]^{2+} = 2[Co^{III}(LS)]^{+}$	-31.0	-15.1

References

[1] a) C. E. Paulsen and K. S. Carroll, *Chemical Reviews* **2013**, *113*, 4633-4679; b) L. E. S. Netto, M. A. de Oliveira, G. Monteiro, A. P. D. Demasi, J. R. R. Cussiol, K. F. Discola, M. Demasi, G. M. Silva, S. V. Alves, V. G. Faria and B. B. Horta, *Comp. Biochem. Physiol. C Pharmacol. Toxicol. Endocrinol.* **2007**, *146*, 180-193; c) N. M. Giles, G. I. Giles and C. Jacob, *Biochemical and Biophysical Research Communications* **2003**, *300*, 1-4.

[2] a) L. Banci, I. Bertini, V. Calderone, S. Ciofi-Baffoni, S. Mangani, M. Martinelli, P. Palumaa and S. Wang, *Proceedings of the National Academy of Sciences of the United States of America* **2006**, *103*, 11814-11814; b) Y. C. Horng, S. C. Leary, P. A. Cobine, F. B. J. Young, G. N. George, E. A. Shoubridge and D. R. Winge, *Journal of Biological Chemistry* **2005**, *280*, 34113-34122; c) T. R. Cawthorn, B. E. Poulsen, D. E. Davidson, D. Andrews and B. C. Hill, *Biochemistry* **2009**, *48*, 4448-4454; d) B. C. Hill and D. Andrews, *Biochimica et Biophysica Acta (BBA) - Bioenergetics* **2012**, *1817*, 948-954.

[3] a) K. Jomova and M. Valko, *Toxicology* **2011**, *283*, 65-87; b) J. T. Pedersen, C. Hureau, L. Hemmingsen, N. H. H. Heegaard, J. Ostergaard, M. Vasak and P. Faller, *Biochemistry* **2012**, *51*, 1697-1706; c) G. Meloni, P. Faller and M. Vasak, *Journal of Biological Chemistry* **2007**, *282*, 16068-16078; d) T. Finkel and N. J. Holbrook, *Nature* **2000**, *408*, 239-247.

[4] a) E. I. Stiefel in *Transition metal sulfur chemistry: Biological and industrial significance and key trends*, *Vol. 653* Eds.: E. I. Stiefel and K. Matsumoto), **1996**, pp. 2-38; b) S. C. Lee, W. Lo and R. H. Holm, *Chemical Reviews* **2014**, *114*, 3579-3600; c) R. H. Holm, P. Kennepohl and E. I. Solomon, *Chemical reviews* **1996**, *96*, 2239-2314; d) C. G. Young, *Journal of Inorganic Biochemistry* **2007**, *101*, 1562-1585.

[5] a) Y. Ueno, Y. Tachi and S. Itoh, *Journal of the American Chemical Society* **2002**, *124*, 12428-12429; b) A. Neuba, R. Haase, W. Meyer-Klaucke, U. Flörke and G. Henkel, *Angewandte Chemie International Edition* **2012**, *51*, 1714-1718; c) A. M. Thomas, B.-L. Lin, E. C. Wasinger and T. D. P. Stack, *Journal of the American Chemical Society* **2013**, *135*, 18912-18919; d) E. C. M. Ording-Wenker, M. van der Plas, M. A. Siegler, S. Bonnet, F. M. Bickelhaupt, C. Fonseca Guerra and E. Bouwman, *Inorganic Chemistry* **2014**, *53*, 8494-8504; e) E. C. M. Ording-Wenker, M. van der Plas, M. A. Siegler, C. Fonseca Guerra and E. Bouwman, *Chemistry – A European Journal* **2014**, *20*, 16913-16921.

[6] M. Gennari, B. Gerey, N. Hall, J. Pécaut, M.-N. Collomb, M. Rouzières, R. Clérac, M. Orio and C. Duboc, *Angewandte Chemie International Edition* **2014**, *53*, 5318-5321.

[7] W.-F. Liaw, C.-K. Hsieh, G.-Y. Lin and G.-H. Lee, *Inorganic Chemistry* **2001**, *40*, 3468-3475.

[8] M. Gennari, D. Brazzolotto, J. Pecaut, M. V. Cherrier, C. J. Pollock, S. DeBeer, M. Retegan, D. A. Pantazis, F. Neese, M. Rouzieres, R. Clerac and C. Duboc, *J Am Chem Soc* **2015**.

[9] O. V. Dolomanov, L. J. Bourhis, R. J. Gildea, J. A. K. Howard and H. Puschmann, *J. Appl. Crystallogr.* **2009**, *42*, 339-341.

[10] G. M. Sheldrick in *SHELXTL-Plus, Structure Determination Software Programs, (Version 6.14.) Bruker Analytical X-ray Instruments Inc.*, *Vol.* Madison, Wisconsin, USA, **1998**.
[11] a) N. Begum, M. I. Hyder, S. E. Kabir, G. M. G. Hossain, E. Nordlander, D. Rokhsana and E. Rosenberg, *Inorganic Chemistry* **2005**, *44*, 9887-9894; b) K. Hou and W. Y. Fan, *Dalton Transactions* **2014**, *43*, 16977-16980.
[12] A. W. Addison, T. N. Rao, J. Reedijk, J. Vanrijn and G. C. Verschoor, *Journal of the Chemical Society-Dalton Transactions* **1984**, 1349-1356.
[13] H. Braunwarth, P. Lau, G. Huttner, M. Minelli, D. Günauer, L. Zsolnai, I. Jibril and K. Evertz, *Journal of Organometallic Chemistry* **1991**, *411*, 383-394.
[14] a) P. J. Pospisil, D. H. Carsten and E. N. Jacobsen, *Chem. - Eur. J.* **1996**, *2*, 974-980; b) A. Berkessel, M. Frauenkron, T. Schwenkreis, A. Steinmetz, G. Baum and D. Fenske, *J. Mol. Catal. A: Chem.* **1996**, *113*, 321-342.
[15] a) W. R. Scheidt, Y. J. Lee, W. Luangdilok, K. J. Haller, K. Anzai and K. Hatano, *Inorg. Chem.* **1983**, *22*, 1516-1522; b) M. M. Williamson and C. L. Hill, *Inorg. Chem.* **1986**, *25*, 4668-4671.
[16] A. De, *J. Crystallogr. Spectrosc. Res.* **1990**, *20*, 279-284.
[17] a) K. Wieghardt, *Angew. Chem. Int. Ed. Engl.* **1989**, *28*, 1153-1172; b) J. Wu, J. E. Penner-Hahn and V. L. Pecoraro, *Chemical Reviews* **2004**, *104*, 903-938; c) S. Blanchard, G. Blain, E. Riviere, M. Nierlich and G. Blondin, *Chemistry-a European Journal* **2003**, *9*, 4260-4268.
[18] M. Mikuriya, F. Adachi, H. Iwasawa, M. Handa, M. Koikawa and H. Okawa, *Bulletin of the Chemical Society of Japan* **1994**, *67*, 3263-3270.